International Journal of Bifurcation and Chaos, Vol. 32, No. 12 (2022) 2230030 (11 pages)

DOI: 10.1142/S0218127422300300

The Influence of Asymmetry on the Dynamics Associated with a Caldera Potential Energy Surface

Matthaios Katsanikas
Research Center for Astronomy and Applied Mathematics, Academy of Athens, Soranou Efesiou 4, Athens, GR-11527, Greece
School of Mathematics, University of Bristol, Fry Building, Woodland Road, Bristol, BS8 1UG, United Kingdom
mkatsan@academyofathens.gr

Malcolm Hillebrand* and Charalampos Skokos†
Nonlinear Dynamics and Chaos Group, Department of Mathematics and Applied Mathematics, University of Cape Town, Rondebosch 7701, South Africa
**m.hillebrand@uct.ac.za*
†*haris.skokos@uct.ac.za*
†*haris.skokos@gmail.com*

Stephen Wiggins
School of Mathematics, University of Bristol, Fry Building, Woodland Road, Bristol, BS8 1UG, United Kingdom
s.wiggins@bristol.ac.uk

Received July 31, 2022; Revised August 9, 2022

In this paper, we analyze the influence of asymmetry on a Caldera potential energy surface. We first study the effect of asymmetry on the structure of the periodic orbit dividing surfaces associated with the unstable periodic orbits of the higher energy index-1 saddles. Then we detect a new type of dynamical matching due to the influence of the asymmetry in the Caldera potential energy surface. Finally, we present the phase space mechanism for this new type of dynamical matching using Lagrangian Descriptors.

Keywords: Periodic orbit dividing surfaces; Caldera potential; phase space structure; chemical reaction dynamics; dynamical astronomy.

1. Introduction

The Caldera-type potential energy surfaces (PES) have been used to describe many organic chemical reactions, such as the vinylcyclopropane-cyclopentene rearrangement [Goldschmidt & Crammer, 1988; Baldwin, 2003], the stereomutation of cyclopropane [Doubleday *et al.*, 1997], the degenerate rearrangement of bicyclo [3.1.0]hex-2-ene [Doubleday *et al.*, 1999; Doubleday *et al.*, 2006] or 5-methylenebicyclo[2.1.0]pentane [Reyes *et al.*, 2002]. This type of PES is characterized by a central minimum and four index-1 saddles (two with high values of energy and two with lower values of energy) that control the transport of the trajectories from

the outer region of the Caldera to the central area or vice-versa (see [Carpenter, 1985; Collins *et al.*, 2014]. The higher energy index-1 saddles are associated with the reactants, and the lower energy index-1 saddles with the products. Similar PES have also been used in dynamical astronomy [Athanassoula *et al.*, 2009].

Until now, all studies concerning the dynamics associated with Caldera-type PES have been carried out with symmetric Caldera PES. These studies have revealed a dynamical phenomenon that has come to be realized of significant importance in organic chemical reactions, termed "dynamical matching" (see [Collins *et al.*, 2014; Katsanikas & Wiggins, 2018]). This phenomenon is based on the fact that *all* trajectories that have initial conditions on the dividing surface of the unstable periodic orbits associated with the higher energy index-1 saddles (where index-1 means there is one positive eigenvalue of the Hessian matrix at this point) evolve straight across the Caldera and exit through the region of the opposite lower energy index-1 saddle. This happens for both higher energy index-1 saddles because of the symmetry of the PES. In terms of a phase space description, this phenomenon is due to the gap between the unstable invariant manifolds of the unstable periodic orbit of the higher energy index-1 saddles and the stable invariant manifolds of the unstable periodic orbits that are in the central area of the Caldera (see [Katsanikas & Wiggins, 2018; Katsanikas *et al.*, 2020a, 2020b]). An extension of this phenomenon to 3D Caldera PES has been studied recently (see [Katsanikas & Wiggins, 2022]) using generalized periodic orbit dividing surfaces (see [Katsanikas & Wiggins, 2021a, 2021b]).

It has been reported that dynamical matching is broken in symmetric Caldera PES in two cases. These cases are:

(1) If the PES is symmetrically stretched in one coordinate direction (see [Katsanikas & Wiggins, 2019; Katsanikas *et al.*, 2020a, 2020b]). In this case, the unstable invariant manifolds of the unstable periodic orbit associated with the higher energy index-1 saddle interact with the stable invariant manifolds of the unstable periodic orbits that exist in the central region of the Caldera, after a critical value of the stretching parameter (see [Katsanikas & Wiggins, 2019; Katsanikas *et al.*, 2020a, 2020b]).

(2) If the critical points of the PES undergo a pitchfork bifurcation, as described in [Geng *et al.*, 2021a, 2021b]. In this case, we have a transition from a potential with the central minimum and four index-1 saddles to a potential with three index-1 saddles (two high energy index-1 saddles and one lower energy index-1 saddle). Dynamical matching is broken as a result of the heteroclinic intersections of the unstable invariant manifolds of the unstable periodic orbits of the higher energy index-1 saddles with the stable invariant manifolds of the unstable periodic orbits of the lower energy index-1 saddle (for details on this transport mechanism see [Katsanikas *et al.*, 2022b]).

In this paper, we will investigate the influence of the asymmetry for a Caldera PES. We will investigate possible changes to the dynamical behavior of the trajectories that have initial conditions on the periodic orbit dividing surfaces of the unstable periodic orbits of the higher energy index-1 saddles. Furthermore, we want to search for possible different types of dynamical matching than what has been observed for the symmetric Caldera PES.

The paper is organized as follows. We describe the model of the asymmetric case of the Caldera potential energy surface in Sec. 2. Then we present the results and our conclusions in Secs. 3 and 4 respectively.

2. Model

The model that we consider is an asymmetric modification of the symmetric Caldera PES introduced in [Collins *et al.*, 2014]:

$$\begin{aligned} V_s(x,y) &= c_1 r^2 + c_2 y - c_3 r^4 \cos(4\theta) \\ &= c_1(x^2+y^2) + c_2 y \\ &\quad - c_3(x^4 + y^4 - 6x^2y^2), \end{aligned} \tag{1}$$

where (x, y), (r, θ) are the position of a test particle in the potential in cartesian and polar coordinates, respectively. We used in our study the same values for the parameters $c_1 = 5, c_2 = 3, c_3 = -0.3$ as in prior works [Katsanikas & Wiggins, 2018, 2019].

In our model we break the symmetry of the potential by adding a term as demonstrated in the following equation:

$$V(x,y) = V_s(x,y) + c_4 x. \tag{2}$$

For the parameter c_4, we used the value $c_4 = 2.5$. This form of Caldera (one central minimum with two upper index-1 saddles to correspond to high values of energy and two lower index-1 saddles to correspond to lower values of energy) is kept for a range of c_4 from 0 to 3. We choose a large value of this parameter in order to investigate clearly the influence of asymmetry. The corresponding Hamiltonian (to which we also refer as the system's energy E) is:

$$H(x, y, p_x, p_y) = \frac{p_x^2}{2m} + \frac{p_y^2}{2m} + V(x, y), \qquad (3)$$

where p_x is the conjugate momentum corresponding to x and p_y is the conjugate momentum corresponding to y, with $m = 1$. Consequently, the Hamiltonian equations of motion are the following:

$$\begin{aligned}
\dot{x} &= \frac{\partial H}{\partial p_x} = p_x, \\
\dot{y} &= \frac{\partial H}{\partial p_y} = p_y, \\
\dot{p}_x &= -\frac{\partial V}{\partial x}(x, y) \\
&= -(2c_1 x - 4c_3 x^3 + 12c_3 x y^2 + c_4), \\
\dot{p}_y &= -\frac{\partial V}{\partial y}(x, y) \\
&= -(2c_1 y - 4c_3 y^3 + 12c_3 x^2 y + c_2).
\end{aligned} \qquad (4)$$

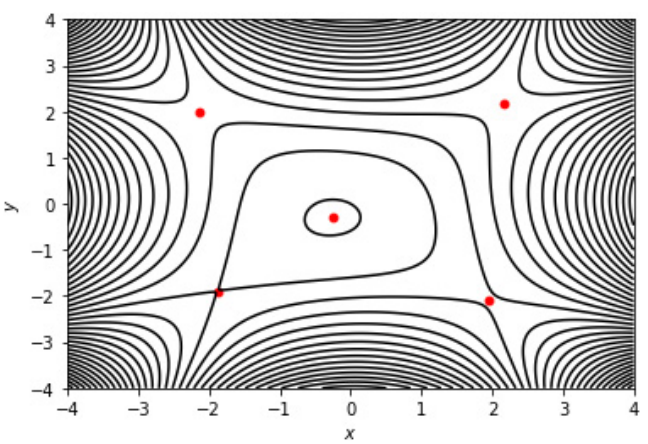

Fig. 1. The contours of the asymmetric Caldera potential (2) with parameters $c_1 = 5, c_2 = 3, c_3 = -0.3, c_4 = 2.5$. We depict the positions of the five equilibrium points (one central minimum and four index-1 saddles around it) using red points.

Table 1. Stationary points of the asymmetric Caldera potential (2) for $c_1 = 0.4$, $c_2 = 3$, $c_3 = -0.3$ and $c_4 = 2.5$.

Critical Point	x	y	E
Central Minimum (CM)	−0.256	−0.304	−0.77
Upper Right Saddle (URS)	2.173	2.161	32.41
Upper Left Saddle (ULS)	−2.125	1.989	21.67
Lower Right Saddle (LRS)	1.963	−2.101	19.63
Lower Left Saddle (LLS)	−1.880	−1.894	10.01

This PES has a central minimum and four index-1 saddles around it (as we can see in Fig. 1), as for the symmetric case of the Caldera PES that was used in [Katsanikas & Wiggins, 2018, 2019], with the only difference that there is no symmetry with respect to the y-axis. The positions of the equilibrium points and the corresponding values of energy are given in Table 1.

3. Numerical Results

In this section, we present our results on the investigation of the influence of asymmetry in a Caldera PES following the discussion above. Firstly, we computed the periodic orbit dividing surfaces associated with the unstable periodic orbits of the higher energy saddles for a value of energy $E = 36$. For this value of energy there are unstable periodic orbits associated with both higher energy index-1 saddle points. The geometric structure of these surfaces and the difference between the periodic orbit dividing surface associated with the unstable periodic orbit of the right higher energy saddle and the periodic orbit dividing surface associated with the unstable periodic orbit of the left higher energy saddle is analyzed in Sec. 3.1. Next we study the trajectory behavior associated with these surfaces in order to investigate the phenomenon of dynamical matching (see Sec. 3.2). The phase space mechanism that is responsible for the trajectory behavior is scrutinized using the method of Lagrangian Descriptors (LDs) (see Sec. 3.2).

3.1. *Periodic orbit dividing surfaces*

In this subsection, we will describe the influence of asymmetry on the structure of the periodic orbit dividing surfaces associated with the unstable periodic orbits of the upper saddles for $E = 36$. The periodic orbit dividing surfaces are $(2n-2)$-dimensional phase space objects in a Hamiltonian system with n degrees of freedom. These surfaces

satisfy the (locally) no-recrossing property and minimum flux. The periodic orbit dividing surfaces are important in the Transition State Theory (TST) [Wigner, 1938; Waalkens *et al.*, 2007]. TST has many applications in chemical reaction dynamics [Wigner, 1938; Waalkens *et al.*, 2007] and dynamical astronomy [Reiff *et al.*, 2022]. The periodic orbit dividing surfaces can be constructed in Hamiltonian systems with two degrees of freedom using the algorithm of [Pechukas & McLafferty, 1973; Pechukas & Pollak, 1977; Pollak & Pechukas, 1978; Pechukas & Pollak, 1979; Pollak, 1985]. The bifurcations of these surfaces have been studied recently in [Katsanikas *et al.*, 2021, 2022a]. A generalization of the periodic orbit dividing surfaces in Hamiltonian systems with three or more degrees of freedom is given recently by [Katsanikas & Wiggins, 2021a, 2021b, 2022]. In this paper, we used the algorithm of [Pechukas & McLafferty, 1973; Pechukas & Pollak, 1977; Pollak & Pechukas, 1978; Pechukas & Pollak, 1979; Pollak, 1985] for Hamiltonian systems with two degrees of freedom as described in [Waalkens *et al.*, 2004; Ezra & Wiggins, 2018; Haigh *et al.*, 2021]:

(1) We compute an unstable periodic orbit.
(2) We project the periodic orbit into the (x, y) subspace (configuration space) of the phase space.
(3) This projection of the periodic orbit is discretized into N points (x_i, y_i) for $i = 1, \ldots, N$ (N is the desired number of points). These points are spaced uniformly according to distance along the periodic orbit. In this paper, we used $N = 1000$.
(4) For every point (x_i, y_i) we compute the $p_{x\,\max,i}$ by solving:

$$H(x_i, y_i, p_x, 0) = \frac{p_x^2}{2m} + V(x_i, y_i). \qquad (5)$$

This equation has solutions if and only if $E - V(x_i, y_i) \geq 0$. If this is true, then the equation has two solutions $\pm p_{x\,\max,i}$(for $E - V(x_i, y_i) > 0$) and one solution $p_{x,i} = 0$ (for $E - V(x_i, y_i) = 0$ — this case is very rare and we have only one value for p_x).
(5) We choose points in the range $-p_{x\,\max,i} \leq p_{x_K} \leq p_{x\,\max,i}$ for $i = 1, \ldots, K$. We obtain p_y by solving the equation $H(x_i, y_i, p_{x_K}, p_y) = E$. In this paper, we used $K = 9$ for the computations in Sec. 3.2, that corresponds to 16 000 points. In this section, we needed more points on the dividing surfaces to analyze their topology in the phase space. For this reason, we used $K = 41$, which corresponds to 80 000 points.

The periodic orbits are the skeletons of these surfaces and they form the 1D boundary of these surfaces. The two upper index-1 saddles have a pair of eigenvalues on the real axis and one pair of eigenvalues on the imaginary axis. This means that the Lyapunov subcenter theorem [Weinstein, 1973; Moser, 1976; Rabinowitz, 1982] guarantees the existence of at least one family of periodic orbits for every index-1 saddle. Every family exists for values of energy above the energy of the corresponding index-1 saddle.

The family of periodic orbits of the upper left index-1 saddle exists for energies above $E = 21.67$ and the family of periodic orbits of the upper right index-1 saddle exists for energies above $E = 32.41$. In the symmetric case of the Caldera PES all families of the upper saddles start to exist above the same value of energy. The first effect of the asymmetry on the Caldera potential energy is that the two families of the upper saddle start from different values of energy. Furthermore, we see that the characteristic curve (the curve that represents the evolution of the initial condition in one direction, in our study the x-direction, in the Poincaré section $y = 2, p_y > 0$ as the energy of the system varies) of the family of periodic orbits of the upper left saddle (ULS) is decreasing (with negative values in the x-direction), as we can see in Fig. 2(a). On the contrary, the characteristic curve of the family of the periodic orbits of the upper right saddle (URS) is increasing (with positive values in the x-direction), as we can see in Fig. 2(b).

The second effect of the asymmetry on the Caldera PES is that the evolution of the stability of the family of the ULS is different from that of the family of the URS. This does not happen for the symmetric case of the Caldera PES. We see in Fig. 3 that the Hénon stability parameter α (see for example, the Appendix of [Katsanikas & Wiggins, 2018] and references therein for more information) of the family of the ULS increases with a very slightly larger slope than that of the family of the URS. Despite this fact, the family of the URS is more unstable due to the consistently larger α values.

Another influence of the asymmetry on the Caldera potential energy surface is the difference in

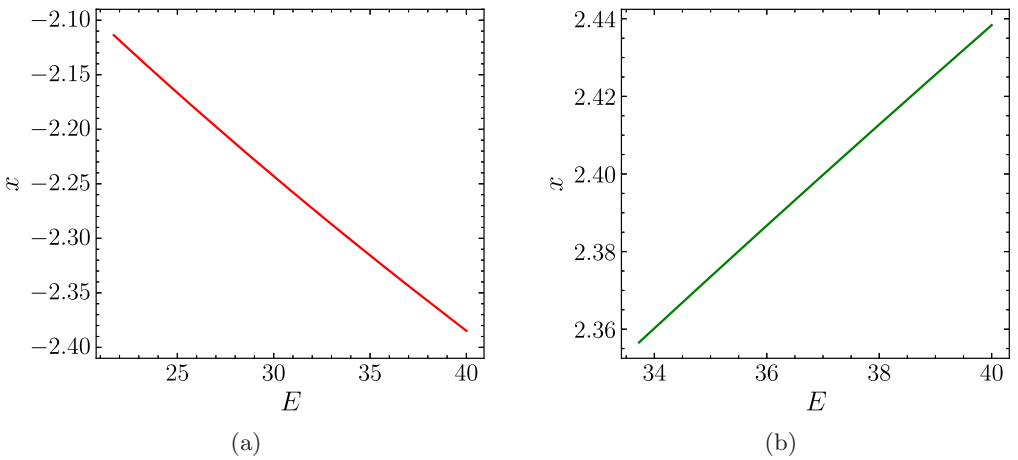

Fig. 2. These diagrams (characteristic diagrams) give the evolution of the x-coordinate on the Poincaré section $y = 2$ with $p_y > 0$ of the families of periodic orbits of (a) upper left saddle and (b) upper right saddle versus energy.

the spatial extent, or *range* of the periodic orbits. This does not occur for the symmetric case of the Caldera PES. As we can see in Fig. 4, the periodic orbits (for $E = 36$) of the two families of periodic orbits of the upper saddles have the same morphology but they have different ranges in the x, y, p_x and p_y directions. We observe that these periodic orbits are curves in the configuration space. The curve that corresponds to the family of the ULS is longer than that of the family of the URS. The range of the periodic orbit of the family of the ULS is in $[-1.65, -2.84]$ and $[1.57, 2.69]$ in the x- and y-directions, respectively. The range of the periodic orbit of the family of the URS is in $[1.92, 2.49]$ and $[1.91, 2.47]$ in the x- and y-directions, respectively. This means that the periodic orbit dividing surface associated with the ULS has larger range in the x- and y-directions than that of the periodic orbit dividing surfaces of the unstable periodic orbits of the URS. This happens because the range of x and y values of a periodic orbit dividing surface is identical with that of the periodic orbit. Furthermore, the periodic orbits of the families of the upper saddles are ellipses in (x, p_x) and (y, p_y) subspaces of the phase space. The green ellipses in Fig. 4, that correspond to the periodic orbit of the URS, are smaller than those that correspond to the periodic orbit of the ULS.

The periodic orbit dividing surfaces associated with the unstable periodic orbit of the upper saddles are ellipsoids in the (x, p_x, p_y) and (y, p_x, p_y) subspaces of the phase space (see for example,

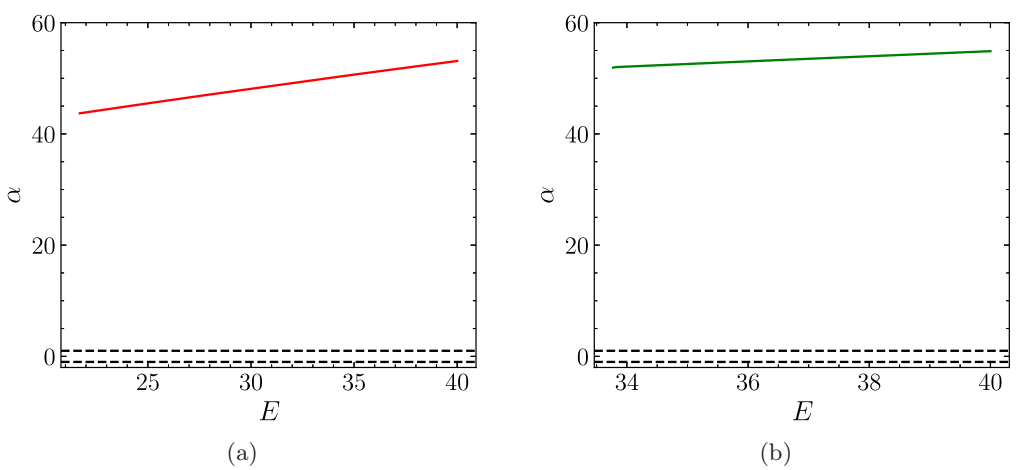

Fig. 3. These diagrams (stability diagrams) give the evolution of the Hénon stability parameter, on the Poincaré section $y = 2$ with $p_y > 0$ of the members of the families of periodic orbits of (a) the upper left saddle and (b) the upper right saddle. The two dashed black lines in each panel represent the axes $\alpha = 1$ and $\alpha = -1$ that distinguish the stability from instability (see text for more details).

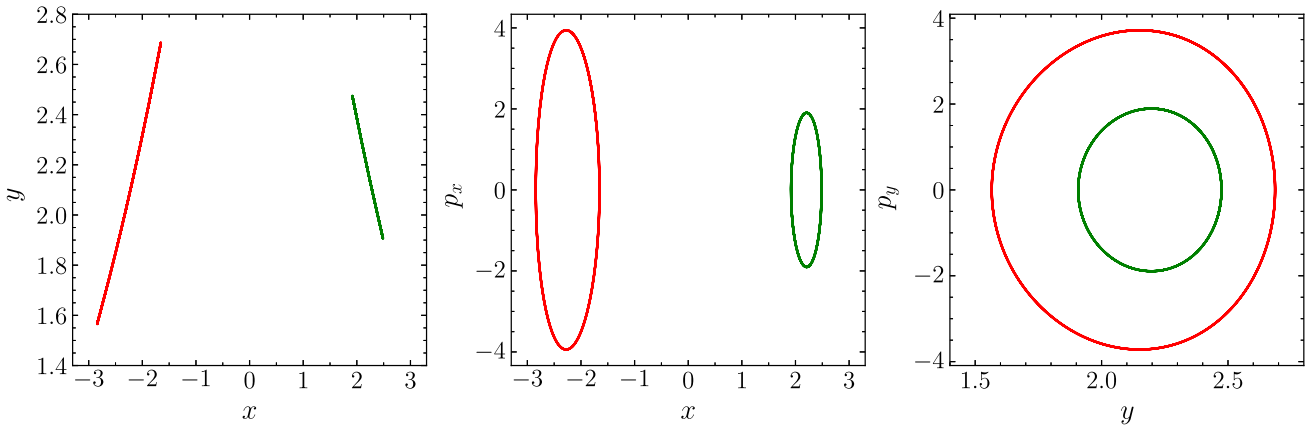

Fig. 4. The representation of the periodic orbits of the upper left saddle (with red color) and of the upper right saddle (with green color) in the (x, y), (x, p_x) and (y, p_y) projections for values of energy $E = 36$.

Fig. 5). In addition, these periodic orbit dividing surfaces are presented as filamentary structures in the (x, y, p_x) and (x, y, p_y) subspaces of the phase space (see for example, Fig. 6). The periodic orbit dividing surfaces associated with the unstable periodic orbits of the ULS have larger range in the p_x- and p_y-directions than that of the periodic orbit dividing surfaces of the unstable periodic orbits of the URS (see (x, p_x) and (y, p_y) projections of the periodic orbit dividing surfaces in Fig. 7). In particular, the range of the periodic orbit dividing surface associated with the ULS has a range in the p_x- and p_y-directions of $[-5.4, 5.4]$ and $[-5.4, 5.4]$, respectively. The ranges of the periodic orbit dividing surface associated with the URS in the p_x- and p_y-directions are $[-2.68, 2.68]$ and $[-2.68, 2.68]$, respectively.

As we described above, the periodic orbit dividing surfaces associated with the unstable periodic orbits of the upper index-1 saddles have similar morphology to each other but different ranges in all coordinates of the phase space. This does not happen in the symmetric case of the Caldera PES. Consequently, the trajectories with initial conditions on the dividing surface with the larger range (the periodic orbit dividing surface associated with the ULS) have a greater probability to visit larger regions of the phase space than the trajectories with initial conditions on the other dividing surface (the

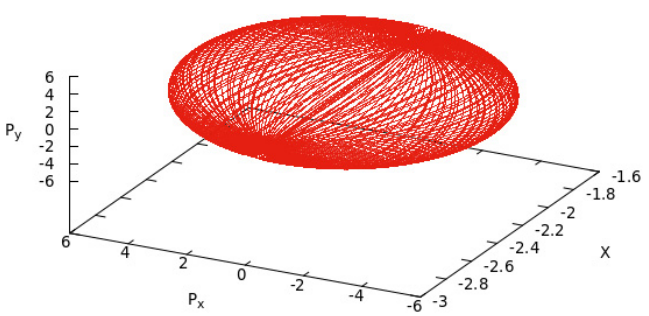

Fig. 5. The 3D projection (x, p_x, p_y) of the periodic orbit dividing surfaces associated with the upper left saddle (with red color) for the energy value $E = 36$.

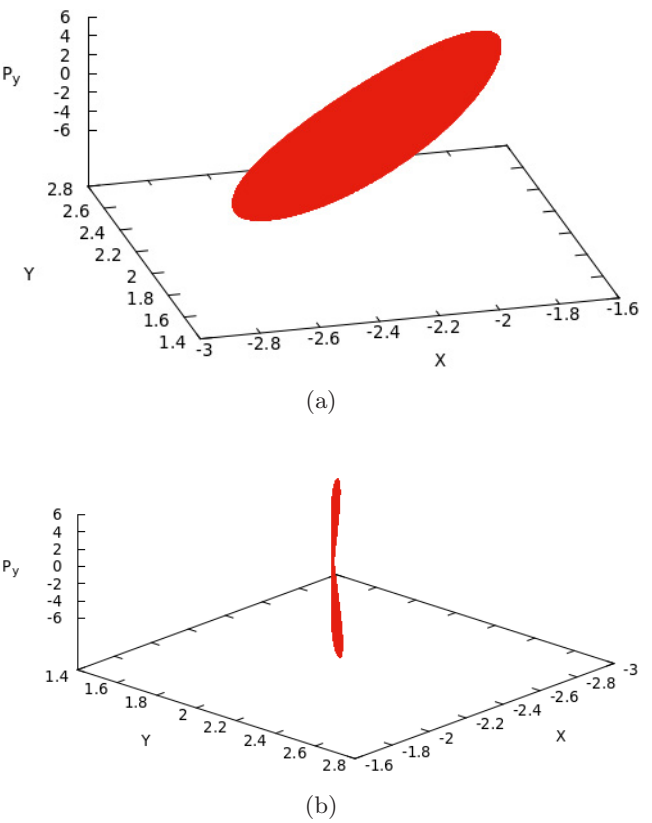

Fig. 6. The 3D projection (x, y, p_y) [using different viewpoints in (a) and (b)] of the periodic orbit dividing surface associated with the upper left saddle for the energy value $E = 36$.

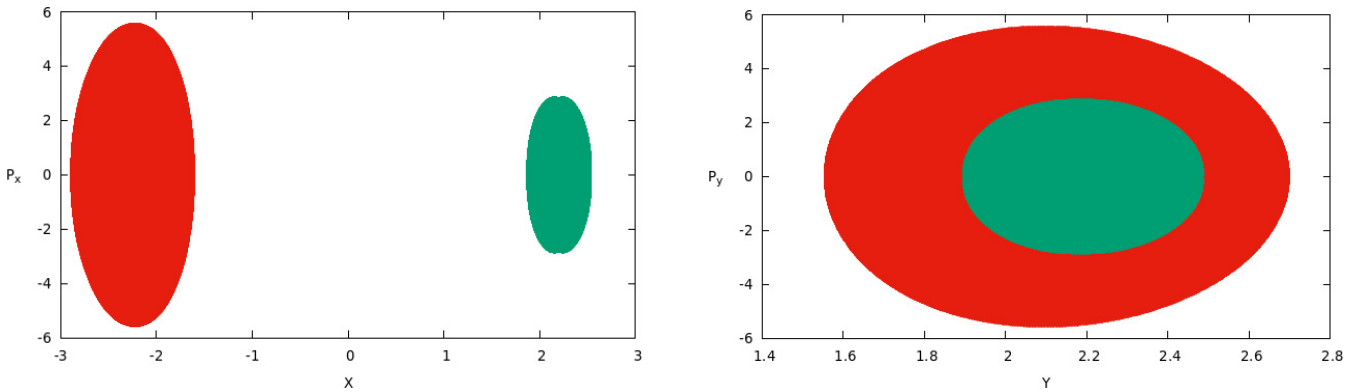

(a) (b)

Fig. 7. The 2D projections (x, p_x) [for (a)] and (y, p_y) [for (b)] of the periodic orbit dividing surfaces associated with the upper left saddle (with red color) and the upper right saddle (with green color) for the energy value $E = 36$.

periodic orbit dividing surface associated with the URS).

3.2. *Dynamical matching*

In this subsection, we will investigate the trajectory behavior associated with the periodic orbit dividing surfaces of the unstable periodic orbit of the upper saddles for $E = 36$, and analyze the origin of this behavior associated with the dynamical matching phenomenon using the results of the previous subsection and the method of LDs (see [Agaoglou *et al.*, 2019; Agaoglou *et al.*, 2020] and references therein). For this purpose, we take a sampling of 16 000 initial conditions using the algorithm that was described in the previous subsection from every periodic dividing surface associated with the unstable periodic orbits of the upper saddles and we integrated them forward and backward in time. The trajectories with initial conditions on both periodic orbit dividing surfaces exhibit two types of behavior:

(1) The trajectories escape directly to infinity (non-reacting trajectories) and they have no possibility to participate in the reaction as they evolve away from the two lower saddles.
(2) The trajectories evolve to the internal region of the Caldera (reacting trajectories) and they may go through the region of one of the lower saddles, which corresponds to chemical reaction.

Now, we see in Fig. 8(b) that *all* the reacting trajectories, with initial conditions on the periodic orbit dividing surface associated with the unstable periodic orbit of the URS, evolve straight across the Caldera and exit through the region of the opposite lower saddle. This is the phenomenon of dynamical matching for the URS. On the contrary, the reacting trajectories with initial conditions on the periodic dividing surface associated with the unstable periodic orbit of the ULS, are trapped in the central area of the Caldera and they exit through the region of *both* lower saddles [see Fig. 8(a)]. Hence, dynamical matching is broken for the ULS. This is a new type of dynamical matching that does not exist for the symmetric cases of a Caldera PES. As we described above, the dynamical matching exists only for the trajectories that have initial conditions on the periodic orbit dividing surfaces associated with one upper saddle and not for both of them.

In order to investigate the origin of this breaking of dynamical matching in the asymmetric case of Caldera PES, we will use the method of LDs. We have already used this method for analyzing the 2D symmetric Caldera PES (see [Katsanikas *et al.*, 2020a, 2020b] — the reader can find details in these references concerning the computation of LDs in a Caldera-type potential).

In Fig. 9, we depict the stable and unstable invariant manifolds using LDs in the Poincaré section $y = 2$ with $p_y > 0$ for $E = 36$. We used this section in order to guarantee the existence of the invariant manifolds of the unstable periodic orbits associated with the upper saddles (the section $y = 2$ is between the y coordinates of the two upper saddles) and their interaction with the invariant manifolds of the central area. We observe in Fig. 9, that we do not have any interaction of the invariant manifolds that are on the right side of the figure (the region of the unstable periodic orbits of the

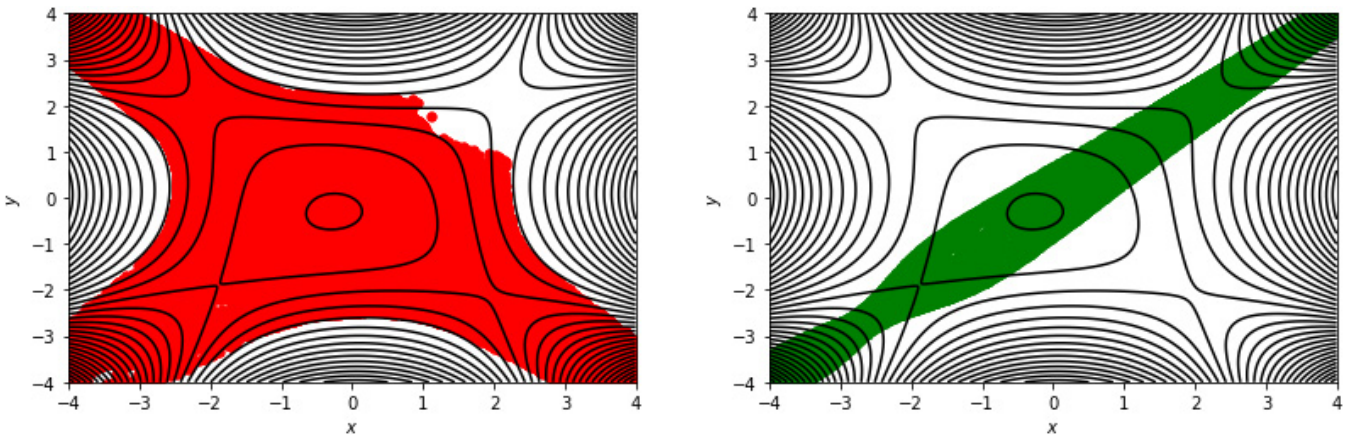

Fig. 8. The trajectories in the configuration space (x, y) with initial conditions on the periodic orbit dividing surfaces associated with the left saddle [with red color — (a)] and the right saddle [with green color — (b)] for the energy value $E = 36$.

URS) with the central area. This means that the invariant manifolds of the unstable periodic orbits of the URS have no heteroclinic intersection with the invariant manifolds of the central area. Consequently, the invariant manifolds transfer the trajectories far away from the central area of the Caldera. It is for this reason that if we take an initial condition close to the region of the unstable periodic orbit of the URS (like the green point in Fig. 9), we have a trajectory that corresponds to dynamical matching [Fig. 10(a)]. This explains the behavior of the trajectories with initial conditions on the dividing surfaces associated with the unstable periodic orbits of the URS [that was described above, illustrated in Fig. 8(b)].

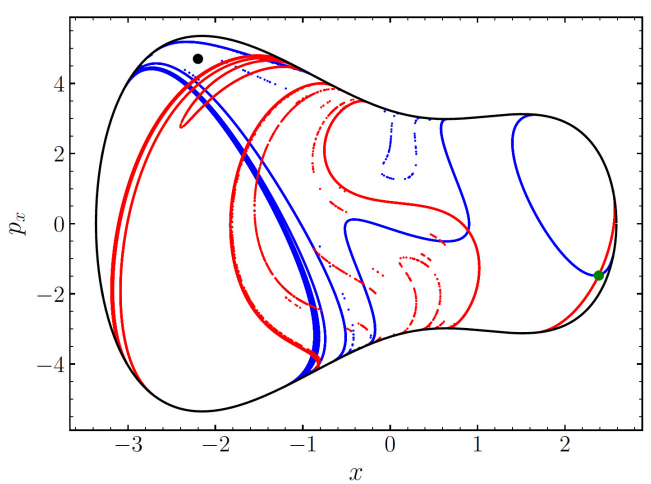

Fig. 9. The stable (blue) and unstable (red) invariant manifolds are extracted (in the 2D slice $y = 2$ with $p_y > 0$) from the gradient of the LDs using $\tau = 4$ for the integration time, for the energy value $E = 36$. We also depict two different initial conditions of trajectories using black and green points, which are depicted in Fig. 10.

We see in Fig. 9 that we have the interaction of the invariant manifolds that emanate from the left side (the region of the unstable periodic orbit of the ULS) with the invariant manifolds that exist in the central area. In particular, we see a black point inside lobes that are formed by the unstable invariant manifolds of the unstable periodic orbit associated with the ULS and the stable invariant manifolds that exist in the central area. This is confirmed by integrating the initial condition corresponding to the black point forward and backward in time [see Fig. 10(b)]. We see that the trajectory moves to the region of the ULS, backward in time and moves to the central area (where it is trapped for some time) forward in time. This means that the lobe is between heteroclinic intersections of the unstable invariant manifolds of the unstable periodic orbits associated with the ULS and the stable invariant manifolds of the central area. This explains the trapping of the trajectories with initial conditions in the region of the ULS. The trajectories initially follow the unstable invariant manifolds of the unstable periodic orbits of the ULS saddle and are trapped in lobes between heteroclinic intersections of these manifolds with the stable invariant manifolds of the central area. Consequently, the trajectories are guided (through these lobes) by the stable invariant manifolds to the central area [see Fig. 10(b)]. Then, according to the second part

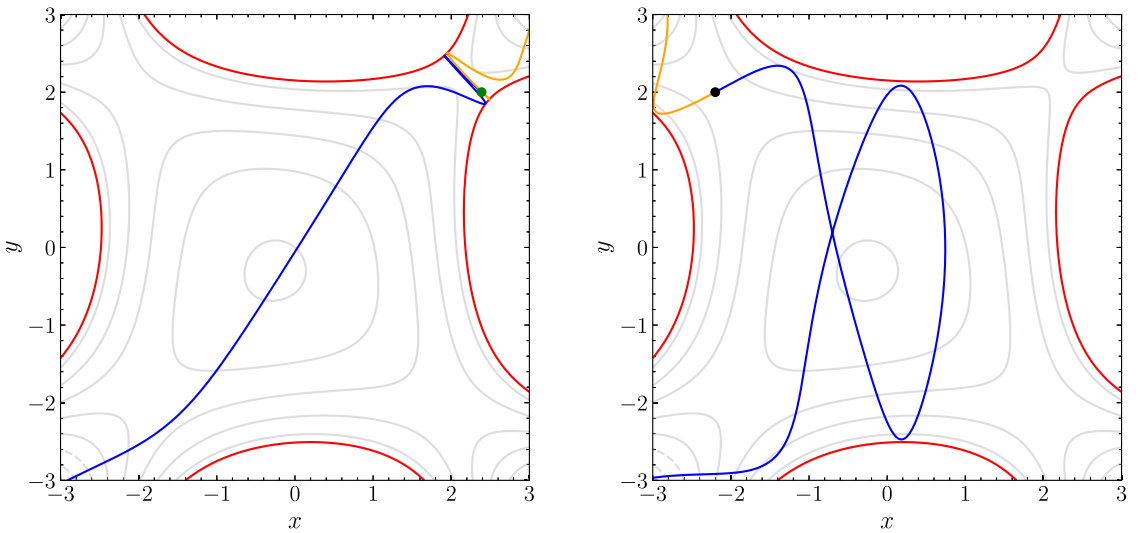

Fig. 10. (a) The forward (blue color) and backward in time (yellow color) evolution in the configuration space (x, y) of the trajectory denoted by a green point in Fig. 9. (b) Similar to (a) but for the trajectory denoted by a black point in Fig. 9. In both panels, red curves depict the boundary of the energetically forbidden region.

of the mechanism of transport that was described in [Katsanikas *et al.*, 2022b], the trajectories are guided from the unstable invariant manifolds of the central area far away from the neighborhood of the unstable periodic orbits of this area and eventually to the exits of the Caldera [like the trajectory of Fig. 10(b)]. As we explained in this paragraph, the interaction of the unstable invariant manifolds of the unstable periodic orbits of the ULS with the central area is responsible for the behavior of the trajectories with initial condition on the dividing surfaces of the unstable periodic orbits of the ULS as described above, and demonstrated in Fig. 8(a).

4. Conclusions

In this paper, we studied the influence of asymmetry on the dynamics associated with a Caldera PES. Our conclusions can be summarized as follows:

(1) One family of periodic orbits associated with the upper index-1 saddles begins to exist for lower values of energy than the other. In addition, the evolution of the stability of the families of unstable periodic orbits associated with the upper index-1 saddle is different for each family.
(2) The periodic orbit dividing surfaces associated with the unstable periodic orbits of the upper saddles have similar morphology to each other, but different ranges in all coordinates of the phase space. This is very important because the trajectories on the periodic orbit dividing surface with the larger range (for a fixed value of energy) can visit larger regions of the phase space.
(3) We detected for the first time a different type of dynamical matching that does not exist in the symmetric cases of Caldera PES. The trajectories with initial conditions on the periodic orbit dividing surfaces of the unstable periodic orbits associated with one upper saddle display a typical behavior of trajectories corresponding to the phenomenon of dynamical matching. On the other hand, we observe the nonexistence of dynamical matching for the trajectories with initial conditions on the periodic orbit dividing surfaces of the unstable periodic orbits associated with the other upper saddle. This is because of the existence or nonexistence of heteroclinic intersections between the unstable invariant manifolds of the unstable periodic orbits of the upper saddles and the stable invariant manifolds of the unstable periodic orbits of the central area of the Caldera.

Acknowledgments

M. Katsanikas and S. Wiggins acknowledge the financial support provided by the EPSRC Grant No. EP/P021123/1. M. Hillebrand acknowledges funding from the National Research Foundation

(NRF) of South Africa, Grant No. 129630. M. Hillebrand and Ch. Skokos thank the High Performance Computing facility of the University of Cape Town and the Center for High Performance Computing of South Africa for providing their computational resources.

References

Agaoglou, M., Aguilar-Sanjuan, B., García-Garrido, V. J., García-Meseguer, R., González-Montoya, F., Katsanikas, M., Krajňák, V., Naik, S. & Wiggins, S. [2019] *Chemical Reactions*: *A Journey into Phase Space* (Bristol, UK, Zenodo), doi:10.5281/zenodo.3568210.

Agaoglou, M., Aguilar-Sanjuan, B., García-Garrido, V. J., González-Montoya, F., Katsanikas, M., Krajňák, V., Naik, S. & Wiggins, S. [2020] *Lagrangian Descriptors*: *Discovery and Quantification of Phase Space Structure and Transport* (zenodo: 10.5281/zenodo.3958985), doi:10.5281/zenodo.3958985.

Athanassoula, E., Romero-Gómez, M., Bosma, A. & Masdemont, J. [2009] "Rings and spirals in barred galaxies–II. Ring and spiral morphology," *Monthly Not. Roy. Astron. Soc.* **400**, 1706–1720.

Baldwin, J. [2003] "Thermal rearrangements of vinylcyclopropanes to cyclopentenes," *Chem. Rev.* **103**, 1197–1212.

Carpenter, B. K. [1985] "Trajectories through an intermediate at a fourfold branch point. Implications for the stereochemistry of biradical reactions," *J. Amer. Chem. Soc.* **107**, 5730–5732.

Collins, P., Kramer, Z., Carpenter, B., Ezra, G. & Wiggins, S. [2014] "Nonstatistical dynamics on the Caldera," *J. Chem. Phys.* **141**, 034111.

Doubleday, C., Bolton, K. & Hase, W. [1997] "Direct dynamics study of the stereomutation of cyclopropane," *J. Amer. Chem. Soc.* **119**, 5251–5252.

Doubleday, C., Nendel, M., Houk, K., Thweatt, D. & Page, M. [1999] "Direct dynamics quasiclassical trajectory study of the stereochemistry of the vinylcyclopropane-cyclopentene rearrangement," *J. Amer. Chem. Soc.* **121**, 4720–4721.

Doubleday, C., Suhrada, C. & Houk, K. [2006] "Dynamics of the degenerate rearrangement of bicyclo[3.1.0]hex-2-ene," *J. Amer. Chem. Soc.* **128**, 90–94.

Ezra, G. S. & Wiggins, S. [2018] "Sampling phase space dividing surfaces constructed from normally hyperbolic invariant manifolds (NHIMs)," *J. Phys. Chem. A* **122**, 8354–8362.

Geng, Y., Katsanikas, M., Agaoglou, M. & Wiggins, S. [2021a] "The bifurcations of the critical points and the role of the depth in a symmetric Caldera potential energy surface," *Int. J. Bifurcation and Chaos* **31**, 2130034-1–11.

Geng, Y., Katsanikas, M., Agaoglou, M. & Wiggins, S. [2021b] "The influence of a pitchfork bifurcation of the critical points of a symmetric Caldera potential energy surface on dynamical matching," *Chem. Phys. Lett.* **768**, 138397.

Goldschmidt, Z. & Crammer, B. [1988] "Vinylcyclopropane rearrangements," *Chem. Soc. Rev.* **17**, 229–267.

Haigh, D., Katsanikas, M., Agaoglou, M. & Wiggins, S. [2021] "The time evolution of the trajectories after the selectivity in a symmetric potential energy surface with a post-transition-state bifurcation," *Regul. Chaot. Dyn.* **26**, 763–774.

Katsanikas, M., García-Garrido, V. J. & Wiggins, S. [2020a] "Detection of dynamical matching in a Caldera Hamiltonian system using Lagrangian descriptors," *Int. J. Bifurcation and Chaos* **30**, 2030026-1–16.

Katsanikas, M., García-Garrido, V. J. & Wiggins, S. [2020b] "The dynamical matching mechanism in phase space for Caldera-type potential energy surfaces," *Chem. Phys. Lett.* **743**, 137199.

Katsanikas, M., Agaoglou, M. & Wiggins, S. [2021] "Bifurcation of dividing surfaces constructed from a pitchfork bifurcation of periodic orbits in a symmetric potential energy surface with a post-transition-state bifurcation," *Int. J. Bifurcation and Chaos* **31**, 2130041-1–16.

Katsanikas, M., Agaoglou, M. & Wiggins, S. [2022a] "Bifurcation of dividing surfaces constructed from period-doubling bifurcations of periodic orbits in a Caldera potential energy surface," *Int. J. Bifurcation and Chaos* **32**, 2230015-1–18.

Katsanikas, M., Agaoglou, M., Wiggins, S. & Mancho, A. M. [2022b] "Phase space transport in a symmetric Caldera potential with three index-1 saddles and no minima," *Int. J. Bifurcation and Chaos* **32**, 2230023-1–9.

Katsanikas, M. & Wiggins, S. [2018] "Phase space structure and transport in a Caldera potential energy surface," *Int. J. Bifurcation and Chaos* **28**, 1830042-1–20.

Katsanikas, M. & Wiggins, S. [2019] "Phase space analysis of the nonexistence of dynamical matching in a stretched Caldera potential energy surface," *Int. J. Bifurcation and Chaos* **29**, 1950057-1–9.

Katsanikas, M. & Wiggins, S. [2021a] "The generalization of the periodic orbit dividing surface for Hamiltonian systems with three or more degrees of freedom — I," *Int. J. Bifurcation and Chaos* **31**, 2130028-1–20.

Katsanikas, M. & Wiggins, S. [2021b] "The generalization of the periodic orbit dividing surface for Hamiltonian systems with three or more degrees of

freedom — II," *Int. J. Bifurcation and Chaos* **31**, 2150188-1–10.

Katsanikas, M. & Wiggins, S. [2022] "The nature of reactive and non-reactive trajectories for a three dimensional Caldera potential energy surface," *Physica D* **435**, 133293.

Moser, J. [1976] "Periodic orbits near an equilibrium and a theorem by Alan Weinstein," *Commun. Pure Appl. Math.* **29**, 727–747.

Pechukas, P. & McLafferty, F. J. [1973] "On transition-state theory and the classical mechanics of collinear collisions," *J. Chem. Phys.* **58**, 1622–1625.

Pechukas, P. & Pollak, E. [1977] "Trapped trajectories at the boundary of reactivity bands in molecular collisions," *J. Chem. Phys.* **67**, 5976–5977.

Pechukas, P. & Pollak, E. [1979] "Classical transition state theory is exact if the transition state is unique," *J. Chem. Phys.* **71**, 2062–2068.

Pollak, E. & Pechukas, P. [1978] "Transition states, trapped trajectories, and classical bound states embedded in the continuum," *J. Chem. Phys.* **69**, 1218–1226.

Pollak, E. [1985] "Periodic orbits and the theory of reactive scattering," *Th. Chem. React. Dyn.* **3**, 123.

Rabinowitz, P. [1982] "Periodic solutions of Hamiltonian systems: A survey," *SIAM J. Math. Anal.* **13**, 343–352.

Reiff, J., Zatsch, J., Main, J. & Hernandez, R. [2022] "On the stability of satellites at unstable libration points of Sun–Planet–Moon systems," *Commun. Nonlin. Sci. Numer. Simulat.* **104**, 106053.

Reyes, M. B., Lobkovsky, E. B. & Carpenter, B. K. [2002] "Interplay of orbital symmetry and nonstatistical dynamics in the thermal rearrangements of bicyclo [n. 1.0] polyenes," *J. Amer. Chem. Soc.* **124**, 641–651.

Waalkens, H., Burbanks, A. & Wiggins, S. [2004] "Phase space conduits for reaction in multidimensional systems: HCN isomerization in three dimensions," *J. Chem. Phys.* **121**, 6207–6225.

Waalkens, H., Schubert, R. & Wiggins, S. [2007] "Wigner's dynamical transition state theory in phase space: Classical and quantum," *Nonlinearity* **21**, R1–R118.

Weinstein, A. [1973] "Normal modes for nonlinear Hamiltonian systems," *Inventiones Mathematicae* **20**, 47–57.

Wigner, E. [1938] "The transition state method," *Trans. Faraday Soc.* **34**, 29–41.